Oxidation protection behaviour of titanium aluminide coatings developed by TIG technique

S. Mridha[1] and T.N. Baker[2]

Department of Mechanical and Aerospace Engineering
James Weir Building
University of Strathclyde, Glasgow G1 1XJ, UK

Email: [1] shahjahanmridha@gmail.com; [2] neville.baker@strath.ac.uk

Keywords: TIG torch, Titanium, Coating, α_2-titanium-aluminide, Dual phase, Oxidation resistance

Abstract

Titanium alloys are attractive in aerospace applications for low density and good mechanical properties but they have poor in oxidation and wear resistance. A coating layer of titanium aluminide can mitigate these problems to some extent and make the alloys suitable for hot structure applications.

This paper discusses the formation of titanium aluminide coatings on commercial purity titanium (CPTi) surfaces by melting a pre-placed aluminium and titanium powder mixture, using a tungsten inert gas (TIG) welding torch. Depending on powder composition and energy input, the resolidified melt layer produced a single phase α_2-Ti_3Al or a dual phase α_2 and γ-TiAl microstructures of lamellar or columnar dendritic types. The microhardness varied from 400 to 600 Hv based on the distribution within the microstructure. Testing the resistance to oxidation, by heating and cooling through nine cycles at 750^0C for a total of 100 h in air, gave a weight gain of 1.00 mg cm^{-2} for the α_2-Ti_3Al coating compared to 2.60 mgcm^{-2} for the CPTi specimen. The dual phase coating showed much improved oxidation resistance with a weight gain of 0.35 mg cm^{-2} after exposure at similar conditions.

INTRODUCTION

Titanium aluminides represent a revolutionary class of an engineering alloys that has been making steady progress since research started in the mid-1970s. These alloys possess structural properties over a serviceable temperature range that competes with those of some nickel-based superalloys [1]. Components that are targeted and have been tested for replacement with titanium aluminides include automotive engine valves, turbocharger rotors, turbine blades, high pressure turbine blade dampers, and the compressor in turbine engines [1-5]. The advantages offered by this class of intermetallics include low density, substantial high-temperature strength, modulus and creep resistance [6]. However, its oxidation resistance is very poor in air or oxygen above 1100 K [7] and it is prone to embrittlement [8]. The limited ductility and formability at room temperature also has precluded its widespread use and application [9].

Although researchers have considered intermetallics for structural applications for over 40 years, it is in the last two decades that most progress has been made [10]. Therefore, intermetallics still represent relatively immature materials that have a significant number of technical barriers that have to be overcome before they could be used as hot section materials, e.g., low creep strength at high temperature and poor ductility at low temperature. Despite the drawbacks, current research has improved the properties of these materials and they are most likely to replace the denser superalloys in less demanding, lower temperature applications. Even then, intermetallics acquire their required mechanical properties at the expense of some of their environmental durability, and will usually require coatings to mitigate a variety of environmental induced problems [11].

The surface layer coating of titanium aluminide can improve the poor wear and oxidation properties of titanium and its alloys for less demanding applications. A wide variety of methods are available for coating, including pack cementation, laser surface alloying and thermal spraying[10].This paper examines the oxidation resistance of titanium aluminide coatings produced by melting preplaced powder mixtures on CPTi surfaces using a TIG torch.

EXPERIMENTAL

CPTi plates (100mm x 30mm x 5mm) were used as the substrates. Titanium powder (99.9% purity, ~50μm size) and aluminium powder (91% purity, ~150 μm size) of ratios given in Table 1, were mixed in a ball mill containing alumina balls. This powder mixture was preplaced on the substrate surface to a thickness of 0.8-1.0 mm using a binder. Details of the powder mixing and placement are described elsewhere [12].

Table 1 Ratio of aluminium and titanium powder mixture.

No.	% wt ratio	% at ratio
1	50Ti-50Al	36Ti-64Al
2	40Ti-60Al	27Ti-72Al

Melting of the preplaced powder was performed using a Miller TIG torch source with a semi-automatic traversing arm. A 2.4 mm tungsten electrode was used to produce the arc in an argon atmosphere with a gas flow rate of 9 L min^{-1}. The current applied for the torch varied between 50-90 A, the electrode height 2- to 4 mm and traverse speed 2 to3 mm s^{-1}. The arc energy density, E was calculated using the formula,

$$E = \frac{IV}{r_B s} \quad (1)$$

where r_B is the arc radius and s is the electrode traverse speed. The technique of determining the arc radius was described previously [12]. The preplaced powder was melted by the torch with energy densities ranging from 127-208 MJm^{-2}.

The microhardness was measured at different depths in the middle regions of the melt cross sections of each track using 200 g load. The error in hardness was ±5%. X-ray diffraction (XRD) and analytical scanning electron microscopy (SEM)-energy dispersive x-ray (EDX) analyses were

performed on the re-solidified surface layer, to identify the phases and aluminium content in the melt structures.

Initially, experiments were conducted to produce single tracks to assess the glazing conditions for the formation of α_2-Ti_3Al and also of dual phase (α_2 and γ-TiAl) structures. Oxidation tests were carried out on overlapped specimens (10mm x 25mm) containing α_2 alone or dual phase structures. Melting of 25% overlapping tracks was used to produce a large coating surface of area 15mm x 30mm. The resolidified layer was ground to produce a flat surface for oxidation testing. An identical sized uncoated CPTi specimen, with similar surface finishing, was used as a reference. These specimens were placed in alumina crucibles, weighed and visually inspected before exposure and after every cycle of heating/cooling in air at 750°C in a muffle furnace, for up to a total of 115 h. A total of nine cycles was undertaken for all the samples. A microbalance of sensitivity 0.10 mg was used for the intermittent weight measurements. After every cycle, the specimens were air cooled for visual inspection and weighing. At the end of the tests, the vertical cross-section of the tested sample was examined in an SEM. To preserve the oxide layer during cutting, the sample was first cold mounted with a low-shrinkage epoxy resin, followed by sectioning using a low speed diamond cutter. A standard technique was used to prepare metallographic samples of the coated transverse sections for microstructural investigation. The polished cross section was etched using Kroll's reagent (3 ml HF, 6 ml HNO_3 and 100 ml H_20).

RESULTS

Microstructure and Composition

Melting of the preplaced powder mixture with 189 or 208 MJm^{-2} energy densities containing 64 at% Al produced the lamellar microstructures. These are seen in Fig.1a for the track glazed at E = 189 MJ m^{-2}, (80A, 2 mm height and 2 mm s^{-1}). The tracks processed with an energy density lower

than 189 MJ m^{-2} produced mostly columnar dendritic microstructures. Lamellar and dendritic microstructures, after glazing over a range of energy densities, have been reported earlier [12].

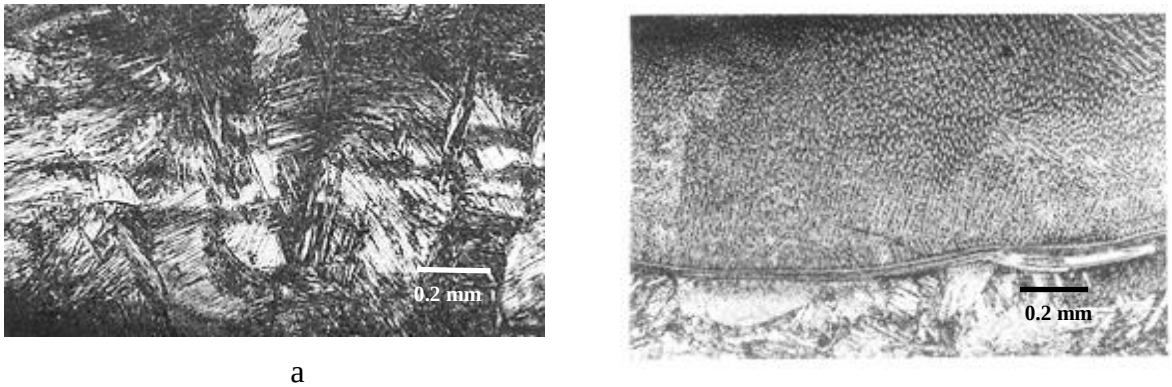

a b

Fig. 1: Micrographs of tracks: (a) 64 at% and (b) 72 at% Al powder mixture and glazed using 189 MJ m^{-2}.

The parallel lamellar structure in Fig. 1a evolved from dendritic growth in preferential directions, and the growth of the grains eventually resulted in their intercrossing. The XRD pattern from this track surface gave predominantly Ti_3Al peaks, together with an α- Ti peak, which indicates that the processing conditions were appropriate for the formation of α_2–Ti_3Al phase. EDX analysis of the platelets gave a composition of 77 at% Ti and 23 at% Al, suggesting Ti_3Al, while the matrix (lamellae) consisted of 89 at% Ti and 11 at% Al (α-Ti). The average Al content of the melt is 15 at%, which corresponds to a structure of α_2 in the Ti-Al phase diagram. It may be noted that the melting of the preplaced powder with overlapping passes has left only about 15 at% Al in the coating, as opposed to 32 at% obtained for a single pass. The decrease in the Al content could be due to the remelting of a portion of the glazed track being overlapped, which caused more loss of Al, coupled with more Ti dilution from melting of base metal.

The coating produced with 72 at% Al powder mixture and glazed at E = 189 MJm^{-2}, resulted in a columnar dendritic microstructure with dendrite growth in the cooling direction (Fig. 1b). The XRD pattern, Fig. 2, shows peaks corresponding to α_2–Ti_3Al, coupled with γ-TiAl peaks. The average Al

content in this structure was 38 at%, which corresponds to the dual $\alpha_2+\gamma$ phase field in the Ti-Al phase diagram.

Energy Density

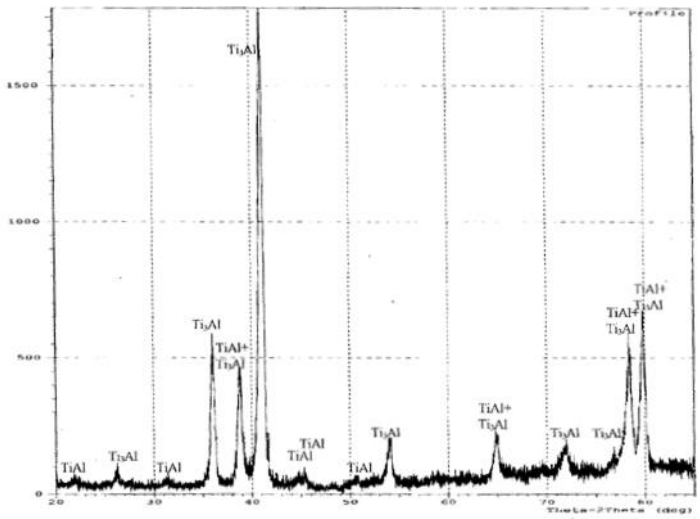

Fig. 2 XRD pattern from the coating with 72 at% Al powder glazed at E = 189 MJm^{-2}.

Hardness

Fig. 3 shows the hardness profile of the specimen containing a lamellar structure of the α_2-Ti_3Al coating. Compared to the base hardness of 180 HV, the microhardness of this coating was found to vary from 400 to 600 HV. The coarse lamellar structure exhibited a hardness between 400-500 HV, while the fine structures had a relatively higher hardness. Fig. 4 records a higher hardness of 500-600 HV, retained to the layer thickness of 1 mm for the columnar dendritic microstructure observed in Fig.1b. The fine dendritic microstructure in this track may be responsible for highest hardness.

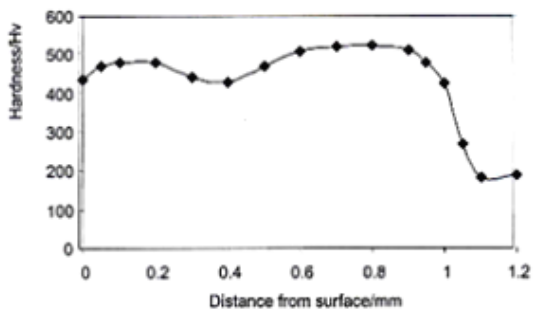

Fig. 3: Hardness profile of lamellar structure track with 64 at% Al and melted at 189 MJm^{-2}

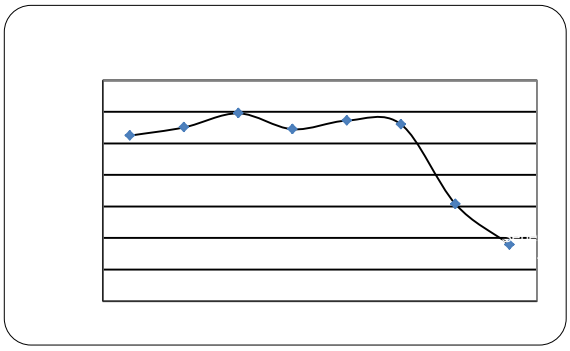

Fig. 4: Hardness profile of the columnar structure track with 64 at% Al and melted at 184 MJm^{-2}

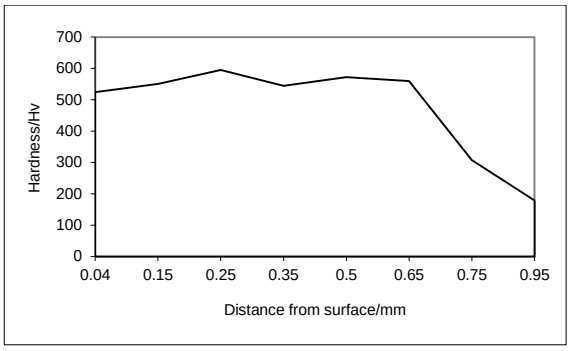

Fig. 4: Hardness profile of the columnar structure track with 64 at% Al and melted at 184 MJm^{-2}

You need to combine the data in both Figs 4

Oxidation Resistance

The oxidation kinetics of both the α_2 coating and that of the reference sample are presented in Fig. 5. The results show identical oxidation reaction kinetics at the initial stage of oxidation for both the coating layer and the reference CPTi alloy. The former levels off after a certain period of heating, where the weight gain for the α_2 coating is less than 50% that of the reference specimen. Fig. 5 further shows that for the α_2 coating, the initial oxidation is faster, followed by a linear rate law and finally slows down to a parabolic growth rate, which is presumed to have been caused after the formation of an oxide layer. On the other hand, the oxidation rate for CPTi is seen to decrease ,but it does not approach parabolic kinetics, and the growth is nearly linear. After heating for 105 h, the reference sample recorded a weight loss, which is considered to be due to spalling of TiO_2, but not of the oxide of interest (Al_2O_3). This was also confirmed by visual inspection, where spallation occurred at several places in the uncoated surfaces. This observation restricts the usefulness of the present technique of oxidation testing for long period of exposure.

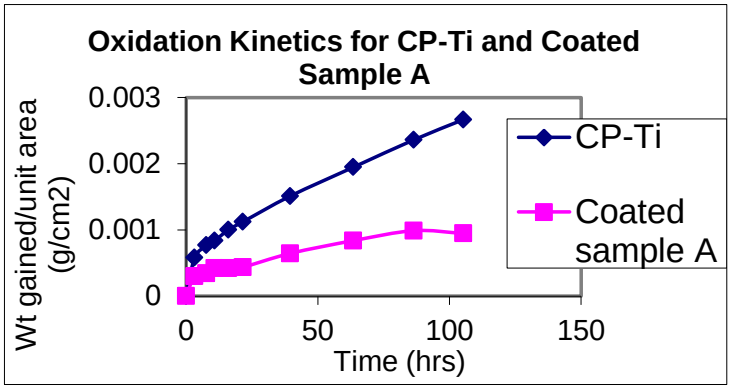

Fig. 5 Oxidation kinetics of the melted layer and CPTi

The cross section of the oxidized specimen seen in Fig. 6 reveals a ~5µm thick oxide layer, O, over a thin white layer, W, with small voids in between the layers. However, the oxide layer is adherent

to the underlying intermetallic coating layer. Below this oxide layer, a large void, V, is present almost continuously.

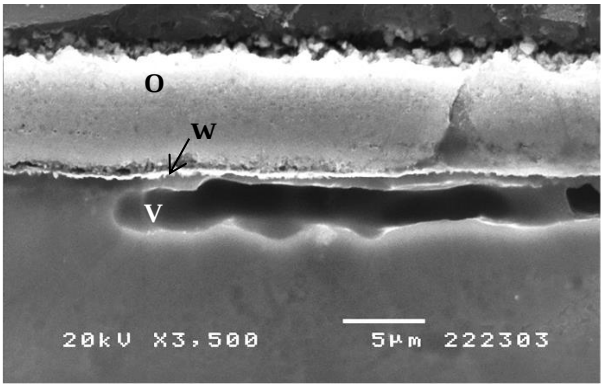

Fig. 6 SEM micrograph of the oxide layer after cyclic oxidation for 105 h at 750°C

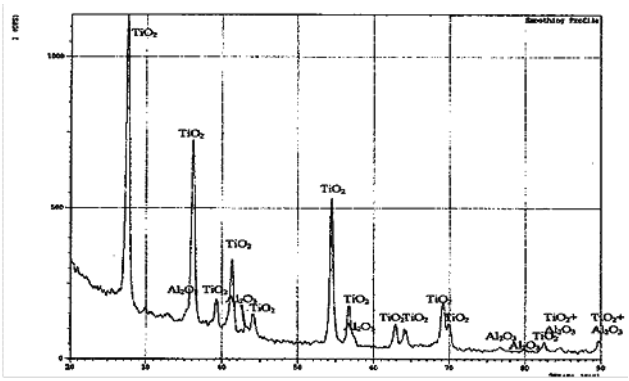

Fig. 7 XRD pattern from the oxide layer at 2° incedence (750°C, 105 h)

The peaks from the oxide layer after 105 h at 750°C, shown in Fig. 7, correspond mainly to TiO_2, with a trace of alumina. The detection of this trace amount of Al_2O_3 is probably due to the insufficient penetration of the GA-XRD. X-ray mapping of a similar section, shown in Fig. 8, gives information on the distribution of these oxides, confirming that the oxide layer contains both TiO_2 and Al_2O_3.

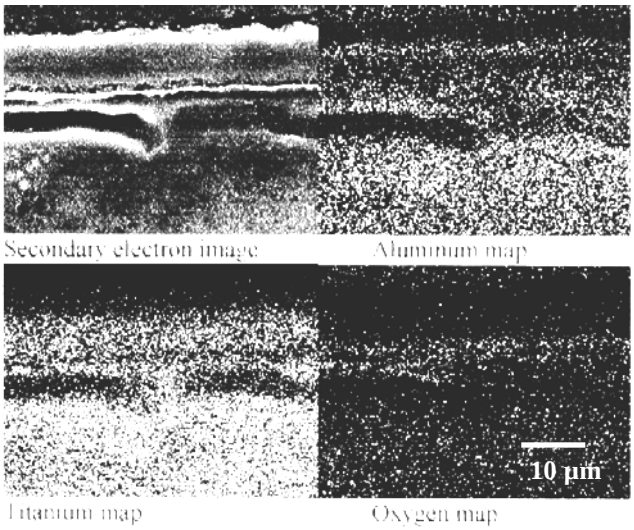

Fig. 8 Distribution of elements in the oxide layer.

Results of the X-ray mapping shown in Fig. 8, verify the formation of thick TiO_2 layer above a thin layer of probably TiN. Al_2O_3 is present throughout the oxide cross-section, but it is concentrated at the surface and near the oxide-metal interface. It is to be noted that a continuous layer of Al_2O_3 protects underlying metal from further oxidation, but a discontinuous Al_2O_3 layer does not fully passivate the metal. In addition to the large void zone, Fig. 8 also shows an aluminium rich zone just below the TiN layer. The voids below the oxide-metal interface are thought to have formed by outward diffusion of titanium atoms from the interface.

EDX line scans for N, O, Al and Ti in Fig. 9, show the distribution of these elements from the surface down to the oxide layer cross-section, after cycling for 105 h at 750°C .These scans show high N peaks just above the metal-oxide interface. The Kα peaks of oxygen and nitrogen are very close and EDX spectrum may lead to erroneous results. Further work needs to be carried out to confirm the presence of a nitride layer beneath the oxide zone.

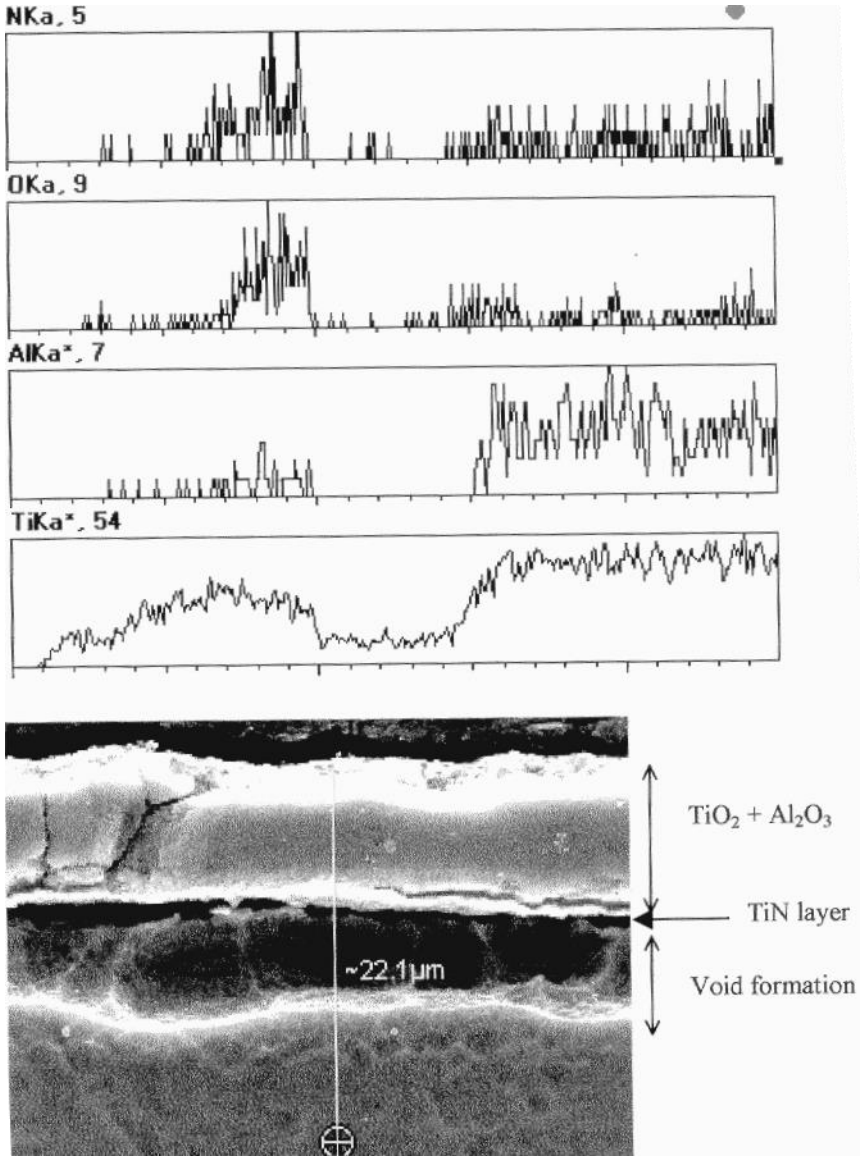

Fig. 9 Line scan across the oxide layer on α_2-coated specimen (left to right) of the element count graph corresponds to traversing from top to bottom of the line on the secondary electron image

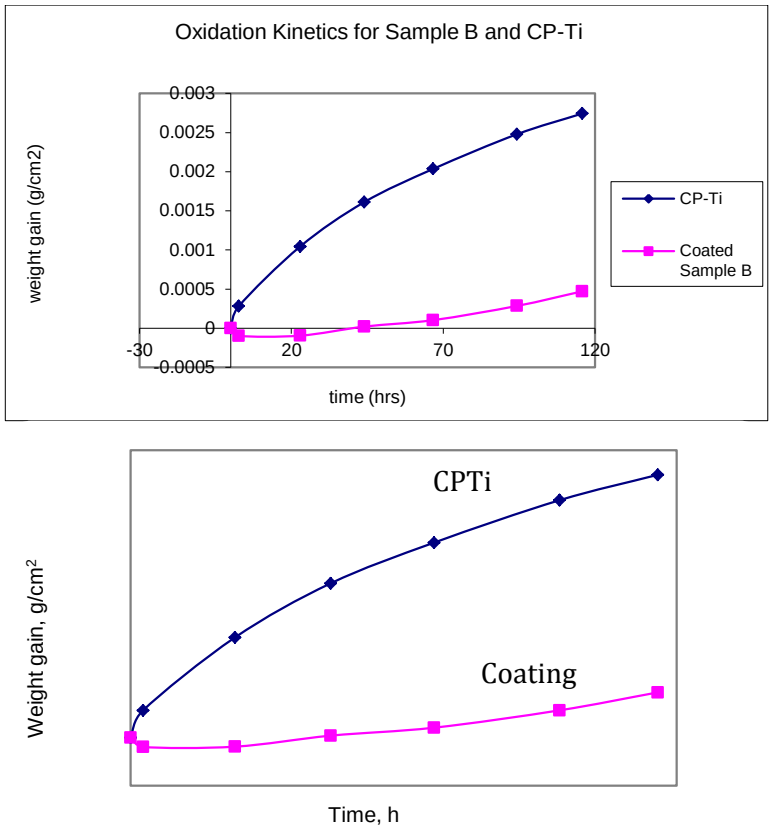

Fig. 10 Oxidation kinetics for the specimen containing dual phase coating along with CPTi

The oxidation kinetics of the specimen containing dual phase $\alpha_2+\gamma$ structures is described from the data in Fig.10, compared with that of the reference CPTi sample. The results clearly show that the dual phase coating has very low oxidation rate compared to that of CPTi. The weight gain due to oxidation of this layer is about 20% that of the reference sample, indicating that the oxidation resistance of the dual phase intermetallic is ~5 times better than CPTi. Comparison with the oxidation resistance of α_2-Ti_3Al structure shown in Fig. 5, indicates that the dual phase structure has a superior oxidation resistance. However, the growth rate appears to be linear and does not level off to a parabolic rate law for the period of testing. Close examination of the oxide layer revealed surface cracking, which propagated down to the metal interface. This cracking may act as fast diffusion paths for oxygen.

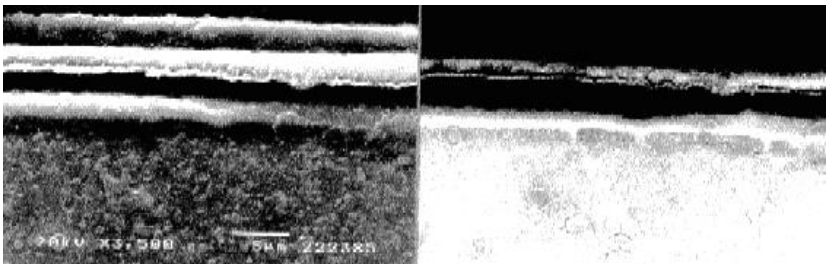

Fig. 11 SE image of dual phase coating (117 h at 750°C): left BSE image showing multilayered oxide; (right) segregation of Al (white line) [Need a µm on the right hand image]

Fig.11 shows layered structure in the oxide cross-section. Segregation of aluminium is also present in the BSE image of the oxide. From the line scan in Fig.11, and X-ray mapping of the oxide cross-section, the top layer was identified as TiO_2, the second layer as a mixture of Al_2O_3 and TiO_2, followed by a void. Such voids could be exaggerated during the hot-mounting of the sample, as the shrinkage of the mount could pull the oxide layer from the metal surface. Below the void, an intermediate layer of TiO_2 was identified, followed by a thin Al rich layer. This could be an Al_2O_3 or TiN layer, similar to the α_2-Ti_3Al coating in Fig. 9, and beneath this is a Ti depleted zone. However, unlike the oxide layer of the α_2-Ti_3Al structure in Fig. 6, there were no voids in the aluminide matrix beneath this oxide layer.

In the X-ray maps, clusters of Al_2O_3 particles have been observed in the coating. In addition, a Ti-deficient region formed below the oxide-metal interface.

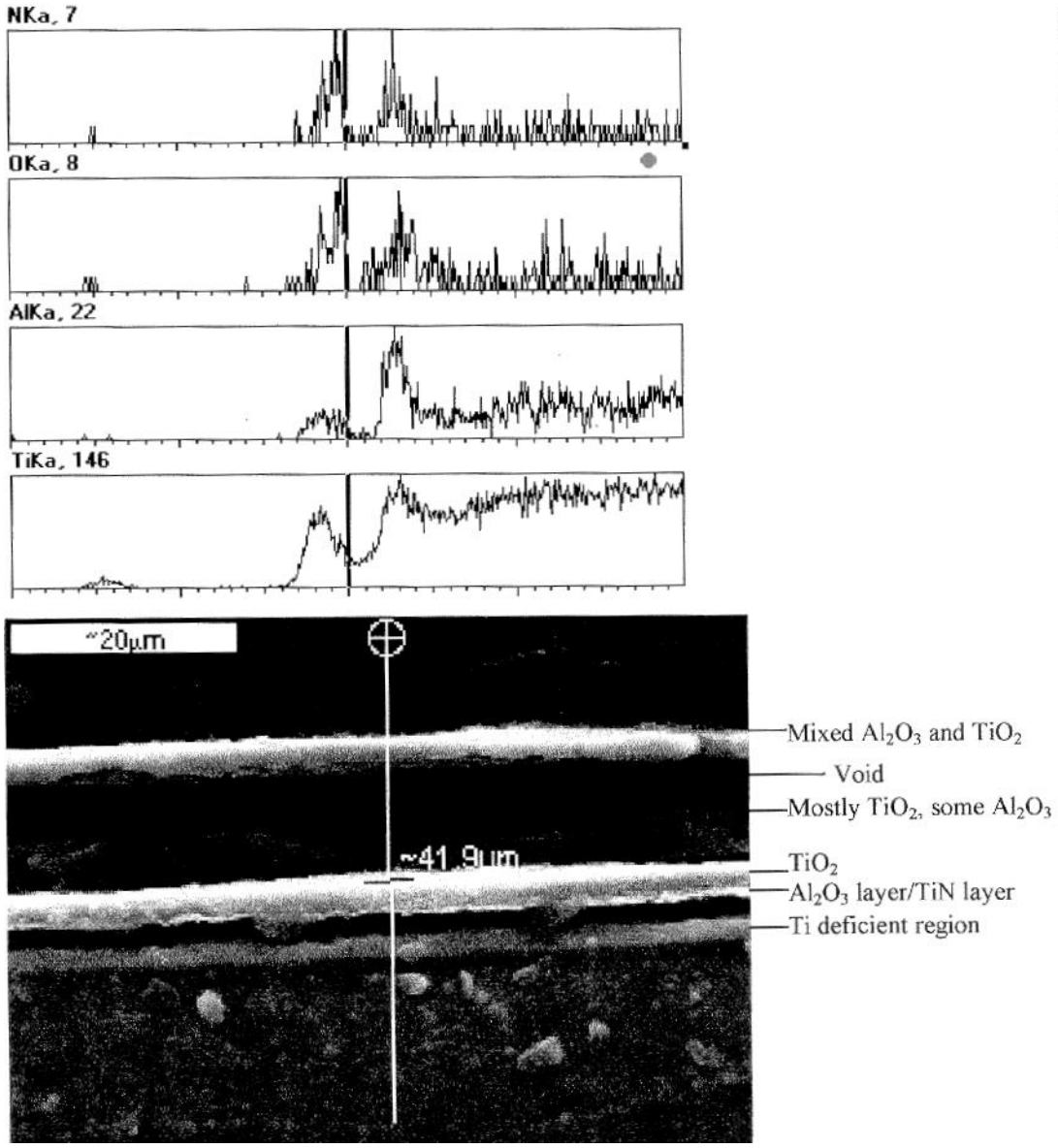

Fig. 12 EDX line scan for different elements across the oxide layer formed on dual phase structure after cyclic oxidation at 750°C for 117 h. Left to right of the element count graph corresponds to traversing from the surface to bottom of the line on the secondary electron image

4 DISCUSSION

4.1 Oxidation Behaviour of α_2-Ti_3Al Coating

The growth of oxide on CPTi following nine cycles of heating to 750°C and holding for 105 hrs, and cooling to room temperature, is non- protective, as shown by the linear rate law after an initial near parabolic growth in Fig. 5. Cyclic oxidation used in this investigation is likely to have created internal stresses because of differential thermal expansions. These stresses are considered to be

responsible for promoting cracking in the oxide layers and then separation from the substrate surfaces. This phenomenon may be related to the oxidation kinetics changing to a linear rate in the later stages. Fig. 13 shows a slight deviation in the linearity of the weight-gain squared against time curve for CPTi. In comparison, the relationship for the α_2-Ti_3Al coating gives a perfect linear fitting, indicating a true parabolic behavior and suggesting a diffusion-controlled growth of the oxide layer on the coated surface.

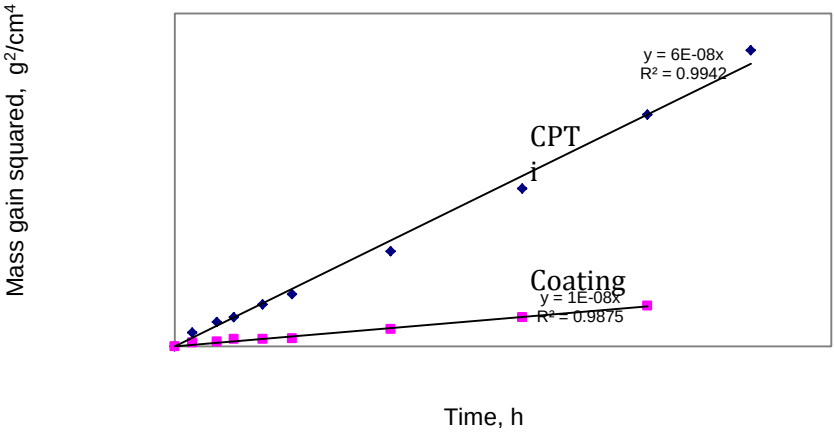

Fig. 13 Plot of weight-gain squared against time for the α_2-coating and the reference sample.

The oxide growth rates of the reference sample and the α_2–Ti_3Al coating determined from Fig. 13 are 6.0 x 10^{-8} $g^2cm^{-4}h^{-1}$ and 1.0 x 10^{-8} $g^2cm^{-4}h^{-1}$, respectively. These figures indicate that the α_2-Ti_3Al coating has an oxidation resistance six times greater than the CPTi material. Although this α_2-Ti_3Al coating has higher oxidation resistance than CPTi, this level of improvement is still considered to be modest. A 15 at% Al content in the coating probably gives such a level of oxidation resistance. The total weight gain of this α_2–Ti_3Al specimen after 100 h heating at 750°C was 1.0 $mgcm^{-2}$, which is comparable to 1.3 $mgcm^{-2}$ for TIMETAL 1100 (Ti-6Al-2.75Sn-4Zr-0.4Mo-0.4Si) exposed under similar conditions [13] and 1.2 $mgcm^{-2}$ for TiAl [14] after exposure of 100 h at 800^0C in air. However, the oxidation test for TIMETAL 1100 was conducted isothermally

while for the present study was cyclic oxidation. The results of the present work demonstrate that the α_2–Ti_3Al coating gives significant improvement in oxidation resistance.

4.2 Oxidation Behaviour of the Dual Phase Coating

For the dual phase coating specimen, the weight gain was 0.35 $mgcm^{-2}$ after 100 h of exposure at 750°C (Fig. 10) and the weight reduction is quite small compared to that of the α_2–Ti_3Al coating given in Fig. 5. This weight gain may be comparable with 0.10 $mgcm^{-2}$ for PtAl coating on IMI834 titanium alloy [14] after 100 h of heating at 800°C, and 0.10-0.20 $mgcm^{-2}$ for sputtered Ti-51Al-12Cr coating on TIMETAL 1100 [13]. The rate constant for this coating [13] could not be determined because of the non-parabolic growth.

The parabolic rate law for the α_2 –Ti_3Al coating in Fig. 13, and linear kinetics for dual phase coating in Fig. 10 determined by the present investigation have some similarities with the results of Shimizu et. al.[15]. They observed linear kinetics after cyclic oxidation of Ti-48 at% Al above 900°C, parabolic kinetics after isothermal oxidation at 800°C or below, which shifted a little towards linear rate after 900^0C. The multi-layered oxide on the dual phase coating was associated with a void space between layers, which were separated under cyclic thermal operation. Their oxide layers [15] had a low weight gain compared to α_2–Ti_3Al coating, and their higher aluminium content may have played an important role in increasing oxidation resistance. The presence of cracks in the oxide layer acted as free paths for inward oxygen diffusion. To assess the oxidation resistance, it is important to consider the weight gain and also the growth kinetics. Linear kinetics are considered to be non-protective.

In some areas, the dual phase coating produced brown coloured oxides, probably of high aluminium content, and slow oxidation kinetics. On the other hand, the α_2–Ti_3Al coating, containing a low aluminium content (15 at%), had a grey coloured rutile-based oxide, showing a faster oxidation rate. The α_2 –Ti_3Al coating formed a single layer oxide scale, which is a mixture of Al_2O_3 and TiO_2.

In contrast, the dual phase coating containing 38 at% Al, gave slower kinetics and produced a multi-layered oxide with Al_2O_3 film, which is considered to be responsible for the reduced oxidation rate. However, this film was not entirely continuous or thick enough to approach Al_2O_3 kinetics. The 38 at% aluminium content in the dual phase may not be enough to develop a thick and continuous Al_2O_3 film. It is reported that the approximate amount of Al needed to form a continuous Al_2O_3 scale is about 56 at% [16]. To obtain a higher oxidation resistant coating, the Al content has to be increased without degrading the adherence of the oxides layers.

5 CONCLUSIONS

- A single-phase α_2-Ti_3Al coating layer was successfully produced on CPTi by melting a preplaced Ti-64 at% powder mixture using TIG torch of energy density 189 MJm^{-2}. The layer microstructure consisted of columnar dendrites with a hardness of 500-600Hv.
- The dual phase coating of titanium aluminide (α_2-Ti_3Al and γ-TiAl) containing 38 at% Al was produced when the preplaced powder mixture contained 72 at% Al was melted at an energy density E = 189 MJm^{-2} or above. The resolidified coating produced lamellar structures with a hardness between 400-500Hv.
- The oxidation resistance of the single phase α_2-Ti_3Al coating was found to be six times higher compared to the reference CPTi specimen tested at 750°C for 100 h in air. The dual phase coating containing higher Al is considered to have much greater oxidation control.

REFERENCES

[1] D.M. Dimiduk: Mater. Sci. Eng. A: 263 (1999), p. 281–288

[2] S. Hurta et.al., in: *Titanium'95: Science and Technology*, edited by P.A. Blenkinsop, W.J. Evans, H.M. Flower, Institute of Materials (1996), p. 97

[3] R.M. Imayev 1, V.M. Imayev 1, M. Oehring, F. Appel: Intermetallics 15, (2007), p. 451-460.

[4] L. Cao, H. W. Wang, C .M. Zou , Z. J. Wei: J. Alloy Compds. 484, (2009), p. 816–821

[5] K. Kothari, R Radhakrishnan, N M. Wereley: Progress in Aerospace Sciences: 55 (2012), p.1–16.

[6] H. Clemens, H. Kestler: Adv. Eng. Mater. **2**, (2000), p. 551 - 570.

[7] D. Kim1, D. Seo, Xi. Huang, T. Sawatzky, H. Saari, J. Hong,Y-W. Kim: Int. Met Revs: 59 (2014), p. 297-325.

[8] G. Welsch and A.I. Kahveci, in: *Oxidation of High-Temperature Intermetallics*, edited by T. Grobstein and J. Doychal, The Mineral, Metals and Materials Society, (1988), p.207

[9] H. Clemens, A. Bartels, S. Bystrzanowski ,H. Chladil, H.Leitner ,G.Dehm ,R. Gerling and F. P. Schimansky: Intermetallics, 14 (2006), p.1380-1385 .

[10] F. Appel, J.D.H.Paul and M. Oehring: *Gamma Titanium Aluminide Alloys: Science and Technology* **(**Wiley, 2011)

[11] C. Leyans, R. Braun, M. Fröhlich and P.E.H. Hovsepian: JOM, 58 (2006), p.17-21.

[12] S. Mridha, H. S. Ong, L. S. Poh and P. Cheang: J. Mater. Process. Technol., 113/1-3 (2001), p. 516-520.

[13] C. Leyens, M. Peters, and W. A. Kaysser, in: *Titanium '95: Science and Technology*, edited by P. A. Blenkinsop, W. J. Evans, H. M. Flower, The Institute of Materials, London, (1995), p.1935-1942.

[14] I. Gurrappa and A. K. Gogia: Surf. Coat. Technol. 139 (2001), p. 216-221.

[15] T. Shimizu, T. Iikubo and S. Isobe: Mater. Sci. Eng. A, 153 (1992), p.602-607

[16] C. Wagner: J. Electrochem. Soc., 99 (1952), p.369

[17] W.J. Quadakkers, A. Elschner, N. Zheng and H. Hickel, in: *Proc. 12th International Corrosion Congress*, NACE International, (1993), p.3842-3850

[18] Y. Murata, M. Morinaga, Y. Shimamura, Y. Takeda and S. Miyazaki, in: *Structural Intermetallics*, edited by R. Darolia et al., The Minerals, Metals and Materials Society, (1993), p.247-256.